Expanding the perspective of polymeric selective contacts in photovoltaic devices using branched polyethilimine

Authors: Eloi Ros*[1], Thomas Tom*[2], David Rovira[1], Julià Lopez[2], Gerard Masmitjà[1], Benjamin Pusay[1], Estefania Almache[1], Isidro Martin[1], Maykel Jimenez[1], Edgardo Saucedo[1], Eva Tormos[2], Jose Miguel Asensi[2], Pablo Ortega[1], Joan Bertomeu[2], Joaquim Puigdollers[1], Cristobal Voz[1]

[1]*Universitat Politècnica de Catalunya (UPC), 08034 Barcelona, Spain,* [2]*Universitat de Barcelona (UB), 08007, Barcelona, Spain,* **equally contribuiting authors*

Abstract

This work studies the use of polymeric layers of polyethylenimine (PEI) as an interface modification of electron selective contacts. A clearly enhanced electrical transport with lower contact resistance and significant surface passivation (about 3 ms) can be achieved with PEI modification. As for other conjugated polyelectrolytes, protonated groups of the polymer with their respective counter anions from the solvent create an intense dipole. In this work, part of the amine groups in PEI are protonated by ethanol that behaves as a weak Brønsted acid during the process. A comprehensive characterization including high-resolution compositional analysis confirms the formation of a dipolar interlayer. The PEI modification is able to eliminate completely Fermi level pinning at metal/semiconductor junctions and shifts the work function of the metallic electrode by more than 1 eV. Induced charge transport between the metal and the semiconductor allows the formation of an electron accumulation region. Consequently, electron selective contacts are clearly improved with a significant reduction of the specific contact resistance (less than 100 $m\Omega \cdot cm^2$). Proof-of-concept dopant-free solar cells on silicon were fabricated to demonstrate the beneficial effect of PEI dipolar interlayers. Full dopant-free solar cells with conversion efficiencies of about 14% could be fabricated on flat wafers. The PEI modification also improved the performance of classical high-efficiency heterojunction solar cells.

Keywords

Dipole, Silicon, solar cells, Fermi Level Pinning, Conjugated polyelectrolyte.

Introduction

Diversifying the available libraries for carrier selective contacts has led to a remarkable breakthrough in crystalline silicon (c-Si) solar cells. It has motivated extensive research as a consequence of its fabrication ease and outstanding device performance.[1,2,3,4] These Electron and Hole Transport Layers (ETLs and HTLs) based on metal oxides, nitrides, alkali/alkaline earth metal salts and organic polymers are capable of silicon surface passivation and allow the elimination of unpleasant effects such as Schottky barriers and Fermi level pinning at the metal-semiconductor interface. 5,6,7,8,9,10 Crystalline silicon solar cells have reported close to

Shockley-Queisser limit efficiencies up to 26.7 %, while simultaneously being a cost-effective technology that occupies 90% of the world photovoltaic (PV) market. However, traditional technologies (e.g. Back Surface Field, BSF, Passivated Emitter Rear Cell, PERC, Heterojunction with Intrinsic Thin layer, HIT, …) suffer from high temperature and complex deposition techniques involving the use of hazardous gases in the fabrication process. Moreover, defects created in the doping process are a cause for parasitic absorption and recombination in the films. [11,12] Some of these disadvantages, including complicated deposition steps have kept the market share of a great performing device such as amorphous silicon HIT heterojunction solar cells limited to the 5%. [13] Nevertheless, doped layers can be replaced by a selective contact film using a broad variety of techniques (e.g. thermal evaporation, sputtering, spin coating, Atomic Layer Deposition, etc.). This idea can help to eliminate high temperature diffusion processes and lead to simple, cleaner and cheaper fabrication processes in silicon solar cells. [14,15]

Carrier selective contacts based on organic molecules have attracted the research due to its highly adjustable electronic and chemical properties and cheaper fabrication process.[16,17] Interfacial layers based on organic molecules have been shown to modify the apparent work function (WF) of metallic electrodes. In this sense, the electric dipole moment of these interlayers has proven capable shifting the electronic band alignment across the interface and therefore the properties of the metal/semiconductor junction[18,19]. Various organic molecules investigated for ETL layers such as conjugated polyelectrolyte poly [(9,9-bis(3'-(N,N-dimethylamino)propyl)-2,7-fluorene)-alt-2,7-(9,9-dioctylfluorene) (PFN), amino acids such as Glycine, Histidine, phenylalanine and HTLs being poly(3,4-ethylene dioxythiophene):poly(styrenesulfonate) (PEDOT:PSS), fluorescent polymers poly(9,9-dioctylfluorenyl-2,7-diyl) (PFO) and lissamine Green B have reported good efficiencies beyond 14% .[20,21,22,23]

The conjugated polyelectrolytes (CP) working principle has been sometimes described to come from the formation of an oriented dipole layer and an associated Helmholtz potential.[24] It is via this potential that energy barriers induced in the surface between a semiconductor and a metal, sometimes due to charge transfer phenomena such as Fermi level pinning, can be modified. [25,26] Branched polyethylenimine (b-PEI) is a cationic polyelectrolyte with a large number of amines. The lone pair of electrons in these amines are reactive enough to modify the electrical properties of the junction. Thereby, inducing chemical and field effect passivation at the semiconductor surface.[27,28]

In this paper we explore the advantages of b-PEI as an electron selective contact, and prospect for a deeper explanation of its working principle involving the conduction mechanisms related to dipole layers (e.g. conjugated polyelectrolytes), as well as their specific effect in Metal/Insulator/Semiconductor junctions (i.e. M/CP/S). Finally, b-PEI is integrated as the ETL in a dopant free crystalline silicon solar cell test structure with efficiencies beyond 14%.

Experimental

Branched polyethylenimine solution (b-PEI) 50 wt% in H_2O, average Mw = 750000 by LS were used as electron selective contact. Polyethylenimine solutions of different weight percentages from 0.1 wt% - 0.0001 wt% were prepared using ethanol as the solvent. All the chemicals were purchased from Sigma-Aldrich.

One-side polished (FZ) n-type c-Si (100) wafers with a thickness of 280 µm and resistivity 2 Ω·cm were used as substrates. All the wafers were treated with a HF dip for 1 min to remove the native oxide from the surface. Spin coating of PEI solutions was performed on silicon wafers at 5000 rpm for 60 s and then the films were annealed at a temperature of 80°C for 2 min on a hot plate in ambient air. The PEI films were deposited on bare silicon and on passivating hydrogenated amorphous silicon (a-Si:H)layers (4 nm) deposited by Plasma Enhanced Chemical Vapour Deposition (PECVD). The thickness of PEI films of various concentrations was measured by ellipsometry. After spin-coating, aluminium (Al) electrodes with a thickness of 300 nm were thermally evaporated using a shadow mask to obtain a transfer-length-method (TLM) pattern. These samples were characterized electrically to determine their contact resistance on n-type c-Si. Quasi-steady state photoconductance measurements were also done to study the effective carrier lifetime of c-Si with spin-coated PEI films. The samples for lifetime measurement were prepared on n-type c-Si wafers with a rear a-Si:H (i/n) stack that provides good reference passivation. On the front side, n-Si/a-Si:H (i)/PEI/Al and n-Si/PEI/Al structures were fabricated for testing. The PEI layers for were spin-coated from 0.01%/0.002 wt% solutions a thin layer of Al (10 nm) was thermally evaporated on the front side of the wafer before the lifetime measurements. The AFM measurements of different concentrations of PEI shown in supplementary information were performed to understand the surface roughness of these films on silicon, all being under 0.3 nm of RMS. The PEI films were spin-coated on a sapphire substrate for transmittance measurement and for energy gap analysis. This was done using a PerkinElmer Lambda 950 UV-VIS-IR spectrophotometer. X-ray photoelectron spectroscopy data of PEI films on c-Si were analysed to identify some important peaks for this work (C1s, O1s and N1s). The change in workfunction caused by the PEI layer was investigated by ultraviolet photoelectron spectroscopy (UPS). Finally, the cross-section of the films was observed by high-resolution transmission-electron-microscopy (HRTEM) to study their morphology.

Device fabrication and Characterization

Silicon solar cells with five different architectures at the rear side contact were developed to study the electron selectivity of PEI films. All these devices were fabricated on non-textured, one-side polished n-type c-Si (100) wafers with a thickness of 280 µm and resistivity of 2 Ω·cm. As a very simple rear contact solution, after an HF dip of 1 min to eliminate the silicon oxide from the surface, the rear side was spin-coated by b-PEI at 5000 rpm for 30 s. Then on the top of the b-PEI layer an Al contact (300 nm) was thermally evaporated. To enhance the passivation and to understand the effect of the b-PEI layer in electron selectivity, an intrinsic (i) a-Si:H and a stack of intrinsic and phosphorus-doped (i/n) a-Si:H layers were deposited in some cells before spin coating the b-PEI layer. The same reference devices without b-PEI layer were also fabricated and analysed for comparison. On the front side, all these devices implemented an innovative hole-selective layer of thermally evaporated vanadium oxide (V_2O_5). The top transparent conductive electrode, as well as the anti-reflection coating, was completed by sputtering of ITO (tin-doped indium oxide). The active area of the solar cells (1 cm^2, 4 cm^2) was defined by photolithography, followed by a wet-etching step for device isolation. Finally, a front contact Ag grid of 2-µm thick was thermally evaporated using a shadow mask. The metallic grid covered 4 % of the active area in the solar cells. The current density-voltage (J-V) electrical characteristics were measured under standard conditions (100 mW/cm^2, AM 1.5G spectrum) using a 94041A solar simulator (Newport, Irvine, CA, USA). Finally, the external quantum efficiency curves were obtained with a QEX10 set-up (PV Measurements, Point Roberts, WA, USA).

Results and Discussion

The contact quality for PEI thicknesses ranging from 0 to 4 nm was studied by the Transmission Line Method (TLM). The polymer was deposited both on pristine c-Si cleaned with HF and on c-Si with a thin intrinsic a-Si:H passivating layer. The results plotted in Fig.1 show that there is a minimum in the specific contact resistance both for the passivated (130 $m\Omega \cdot cm^2$) and non-passivated samples (80 $m\Omega \cdot cm^2$). The optimum thickness values that minimize the contact resistance are about 0.4 and 1 nm, respectively. On one hand, the rapidly increasing specific contact resistance of the non-passivated sample beyond 1 nm suggests electron tunnelling as a dominant conduction mechanism. Such a strong dependence on thickness is also observed in other selective contacts such as alkali salts (e.g. MgF_2, LiF). [29,8] On the other hand, the increase in specific contact resistance under 1 nm indicates at least a secondary mechanism arising at close to monolayer thickness. The passivated sample behaves similarly, though the contact resistance increases more rapidly out of the optimum thickness.

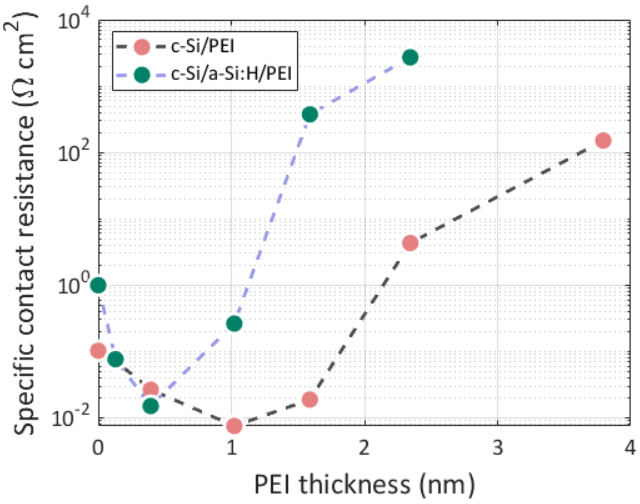

Figure 1. Specific contact resistance as a function of b-PEI thickness.

Quasi Steady State Photo Conductance (QSSPC) study has been performed on different test structures (*see Fig. 2)* for the optimum thickness deduced from TLM measurements. The minority carrier lifetime for both bare and passivated c-Si samples remained practically unchanged after PEI deposition. However, a strong increase by one order of magnitude was observed after depositing a thin semi-transparent aluminium capping (i.e. < 10 nm). The lifetime values were finally higher than 400 µs and approached 3 ms for the samples without and with a-Si:H passivation, respectively. These experiments agree in order of magnitude with lifetime values reported in other works for similar c-Si/PEI/Al structures[28]. Furthermore, the excellent lifetime achieved with a thin 5 nm a-Si:H passivating layer agrees with the V_{oc} value achieved in similar HIT test structures[27].

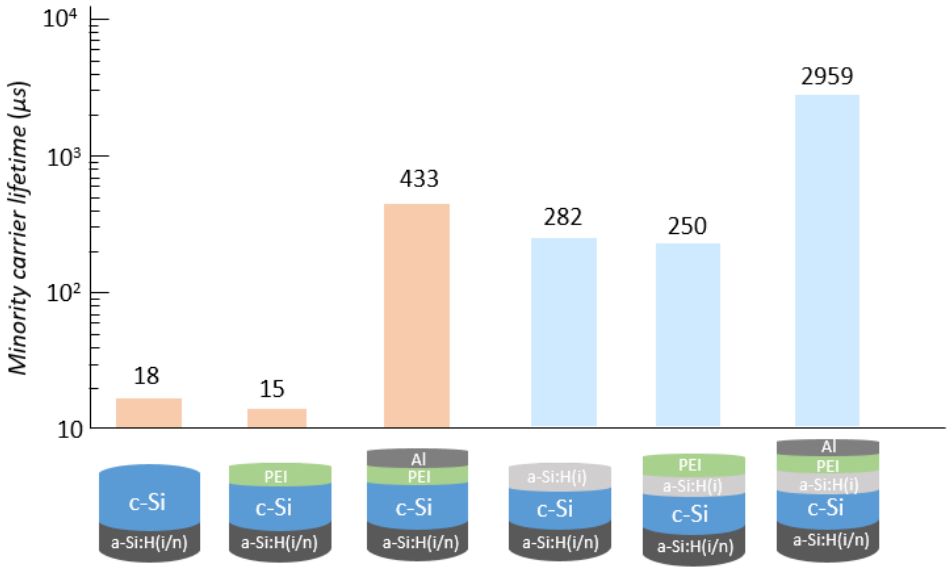

Figure 2. Minority carrier lifetime at 10^{15} cm^{-3} injection for bare silicon and passivated silicon with/without the PEI layer, and with/without a semi-transparent aluminium contact.

The strong lifetime increase with a semi-transparent Al layer indicates an important role of the metallic electrode to improve surface passivation. These results contrast with the lifetime degradation often observed after depositing metallic electrodes on silicon. Our interpretation of this behaviour suggests the formation of a 'Metal/Dipole/Semiconductor' (MDS) junction, a specific variant of classical Metal/Insultator/Semiconductor (MIS) structures. In particular, the explanation considers PEI monomers behaving as cationic conjugated polyelectrolytes with quaternized amine groups. In this hypothesis, amine groups from the polymer protonate in solution acquiring charge. This could be due to PEI high Lewis basicity, simultaneously adhering a charged counter-ion from the solution (i.e. counter-ion condensation),[30] in our case this would be ethanol, which is known to behave as a weak Brønsted acid forming an ethanolate radical. This leads to a picture where the conjugated polyelectrolyte does not have a net charge, but instead forms an interfacial dipole. As a consequence, there is not an electric field nor any charge transfer to the silicon surface. Therefore, minority carrier lifetime is not significantly affected after PEI deposition. The situation changes when a thin Al layer is evaporated onto the conjugated polyelectrolyte. Since the interface dipole effectively reduces the WF of the metal,[31] the aluminium layer behaves as an electron reservoir in contact with silicon. Electron doping by charge-transfer from the metal would primary fill interface traps depinning the Fermi level. The leftover charge results in electron accumulation at the semiconductor surface in a similar manner to the creation of ohmic contacts by the use of low WF metals. The UPS spectra of samples with a PEI capping (see Fig. 3) confirm a decrease in the silicon WF associated to the interface dipole. In this case the measured WF value of reference silicon (i.e. 4.2 eV) differs by 0.84eV to the c-Si/PEI sample (i.e. 3.3 eV). The observed relative displacement is quite similar to the values reported in the literature (ΔWF~ 1.2 eV)[27,28] with slight differences that could be attributed to the different technological procedures. The UPS spectrum for the c-Si/PEI/Al structure indicates an even lower WF value of 2.49 eV, which could account for the charge-transfer and induced band-bending at the silicon surface. As a consequence of such charge-transfer, the internal electric field could further promote dipole orientation in the PEI layer. This result along with QSSPC measurements reinforces the

important role of the metal in the final performance of the structure as an electron-selective contact. Finally, analysis of UPS spectra also reveals an influence from the solvent used in the process. In comparison to the use of ethanol, the solution of PEI in methanol led to an additional 0.15 eV shift in the WF value.

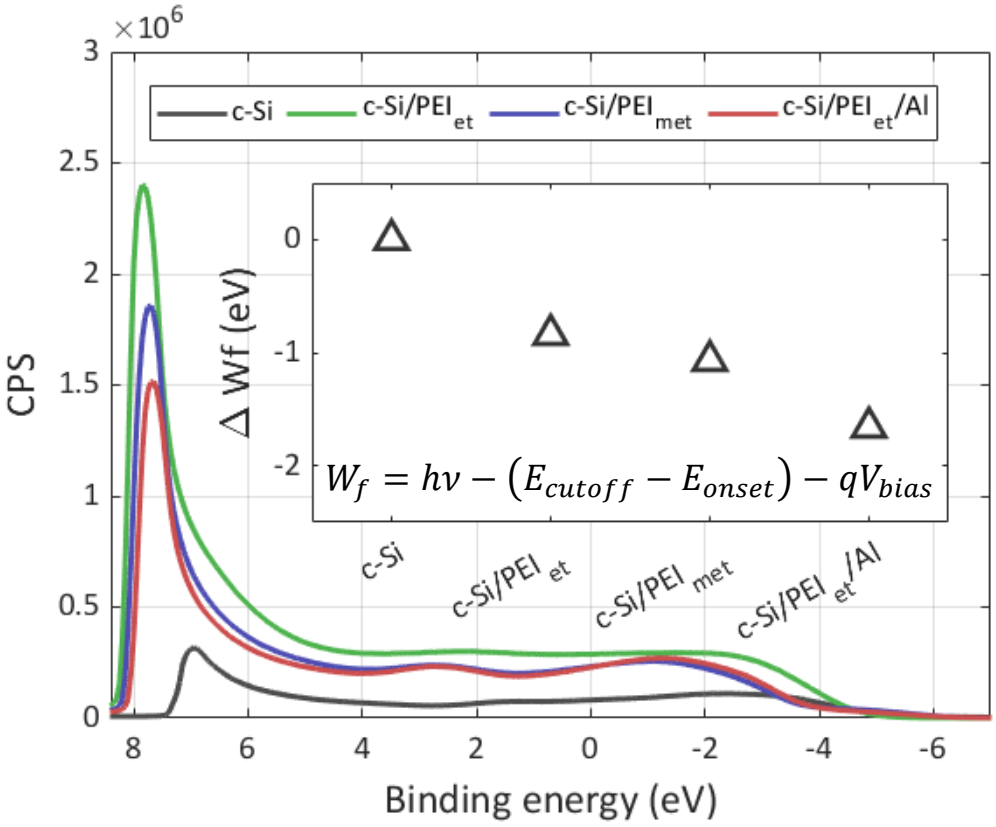

Fig (3) – UPS spectrum for reference c-Si, c-Si/PEI in ethanol solution, c-Si/PEI in methanol solution, c-Si/PEI/Al in ethanol solution. Work function shift for the different structures represented in an inset. Equation used for the calculation of the workfunction can be seen in the graph where $qV_{bias} = 10eV$

Compositional analysis can shed some light to the origin of the dipoles in the PEI layer and explain this phenomenon. The XPS peaks (Fig. 4) of a PEI solution in ethanol indicate the presence of sp^3 hybridized nitrogen that would correspond to quaternized (i.e. protonated) amino groups. Carbon-oxygen bonds are also resolved in the C1s spectrum, which could be related to the presence of leftover solvent (i.e. ethanol) and derivatives. Presence of leftover solvent in a spin coated film is not an unusual phenomenon.[32,33] Presence of C-O signal is also consistent with the initial hypothesis of ethanol behaving as a Brønsted acid in presence of PEI as a Lewis base. The protonated amino groups remain then electrostatically bound to the negative ethanolates, which would be part of the solvent that is not evaporated in the annealing step. The electronegativity of oxygen provides a negative charge density in the –OH group that increases in the ionic ethanolate form.

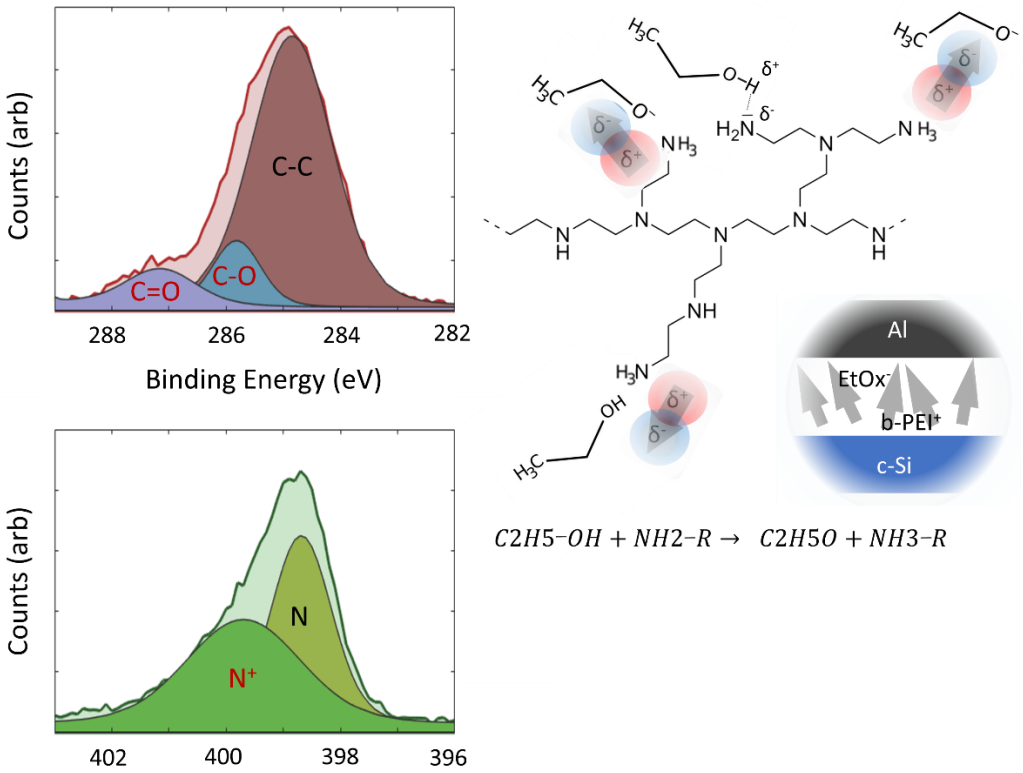

Fig (4) – XPS results of C1s and N1s spectra and scheme of PEI dipole formation

Presence of a double carbon-oxygen bond in the C1 XPS spectrum could be a sign of the alcohol oxidation into the corresponding aldehyde (i.e. ethaldehyde). This would be in line with the idea that ethanol is indeed protonating the amino groups of PEI. As a secondary reaction, some of the resulting ethanolates might thermalize to their aldehyde. Since both ionic groups in PEI^+ and $EtOx^-$ fulfill the octet rule, they can bind electrostatically to form an array of dipoles along the polymer chain. Such dipoles consist of quaternized amine groups and their counter-ion, which is a common phenomenon also observed in other conjugated polyelectrolytes.[34,20], In this sense ethanol has a larger pkA than methanol, i.e. it is a weaker Brønsted acid compared to methanol. Therefore, less protonated amino groups are expected to form in ethanol solutions. Consequently, a less dense dipole layer would explain the 0.15 eV difference in work function shift with respect to methanol solvent observed by UPS.

A carbon and oxygen-rich layer of less than 1.5 nm may be resolved by EDS in the corresponding HRTEM image for the Al/PEI/c-Si MDS junction as seen in Fig(5). A slightly reduced thickness by approximately 0.5 nm is observed in HRTEM images compared to ellipsometry measurements. This difference could be a consequence of using different sides of the silicon wafers (i.e., mechanical, and chemical polishing) for these experiments. The oxygen signal localized in the layer of PEI is consistent with XPS results and it would confirm the presence of leftover solvent within the layer. XPS results evidenced both single and double

carbon-oxygen bonds that we have related to the formation of ethanolate and aldehyde groups after ethanol loses its proton.

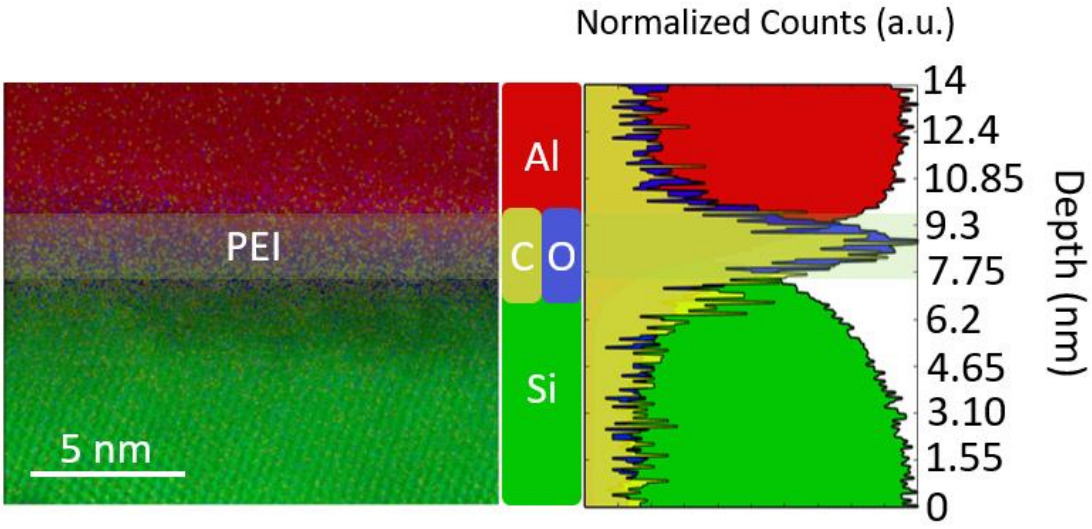

Fig (5) – HRTEM image superimposed with EDS signal of Aluminium Silicon Carbon and Oxygen and depth profiles for each signal along the junction

Spatial distribution of the different elements could bring information on how charge is distributed at the interface. This would confirm whether a dipole layer is indeed formed and it can be considered to explain the operation of conjugated polyelectrolytes. Such a high spatial resolution can be achieved by EELS analysis combined with HRTEM images (Fig. 6). The analysed cross-section of the junction 11 nm deep and 5 nm wide localizes oxygen, carbon, and nitrogen in the same region of carbon and oxygen EDS signal. Nitrogen signal could not be resolved by EDS in the organic interlayer. While it was also difficult to detect by EELS, a Gaussian-shaped peak localizes nitrogen between silicon and the aluminium contact. Similar peaks are also measured for both oxygen and carbon elements. The standard deviation for the carbon peak is the largest at 1.66 nm, while for oxygen and nitrogen peaks they are respectively 1.23 nm and 1.12 nm. This indicates a wider distribution of carbon across the interface compared to nitrogen and oxygen signals. However, the most interesting feature of these fittings is the location of the gaussian peaks. The mean values of carbon and oxygen peaks practically overlap at $\mu_C = 7\ nm$ and $\mu_O = 6.93\ nm$ with less than 1% relative difference. On the other hand, the nitrogen peak located at $\mu_N = 6.2\ nm$ is further apart with a relative difference of 10% with respect to the oxygen peak. This calculation shows that the oxygen and nitrogen peaks are shifted by approximately 7 Å. These results combined with the XPS analysis provide an image of the dipole formed within the layer (Fig 7). According to this scheme, dipoles are originated in PEI layers by protonation and solvation of the amine groups. Furthermore, dipoles are somehow oriented along the polymer chain to form a bilayer of positive and negative charge density that can be resolved by EELS. Such self-assembling could be an effect of the substrate and it seems also enhanced by the metallic contact, as deduced from UPS and QSSPC measurements. The charge density separation in the bilayer is minimal and close to 7Å, in agreement with the thickness of the layer estimated by HRTEM. This work supports that conjugated polyelectrolytes and particularly PEI operate as selective contacts by forming an interface dipole layer between the semiconductor and the metallic contact. This structure can be well defined as a Metal/Dipole/Semiconductor (MDS) junction. The effect of the interfacial dipoles is a modification of the work function of the substrate, hich has been

confirmed by UPS. The displacement of the valence band observed by XPS also points to electron accumulation, because of the work function modification. This electron accumulation improves the operation of the MDS junction as an electron transport layer.

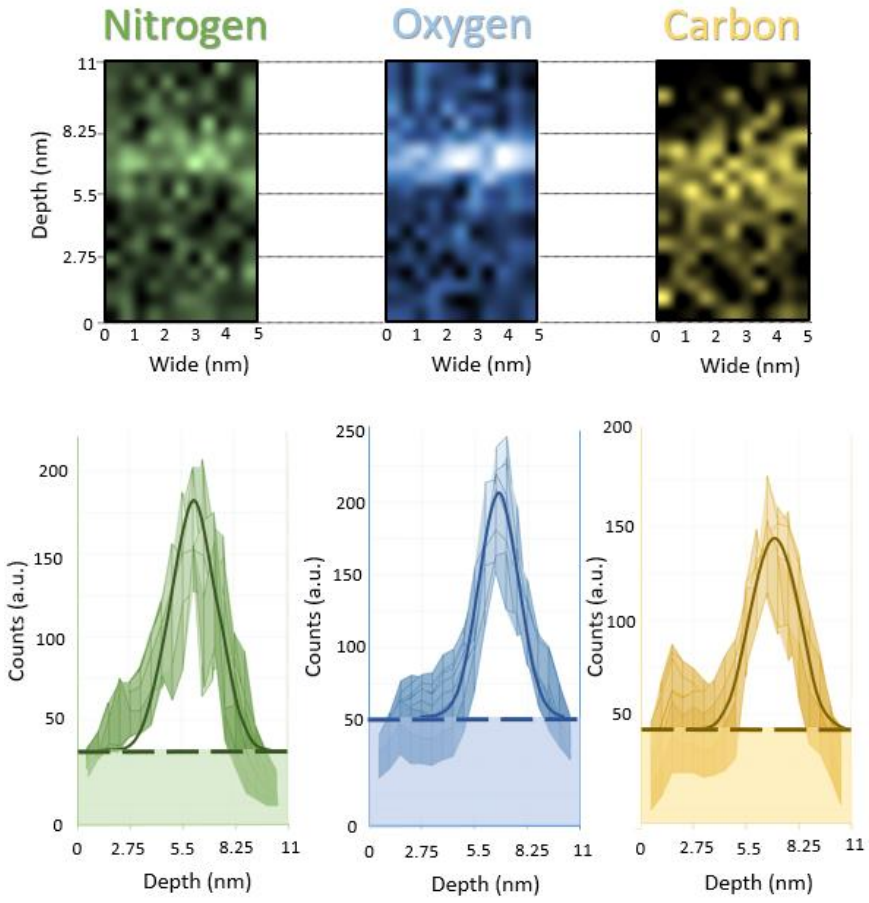

Fig (6)- EELS image for Nitrogen Carbon and Oxygen and 2D mesh plot seen from side section with fitted gaussian profiles

Following, the PEI-modified cathodes were used in a proof-of-concept dopant free solar cell. As introduced before, for the top hole-selective contact we used vanadium oxide that has been widely studied by our group[35].The studied structures include the use of PEI in dopant-free solar cells with selective contacts and to improve standard n-doped a-Si:H ETL structures. Photovoltaic parameters obtained are summarized in Table 1. Figure 8 shows the JV curves under 1.5 AM illumination of the fabricated devices and their corresponding power density electrical characteristics. The solar cells with an aluminium/silicon direct contact show rather low efficiency with a very poor open circuit voltage (V_{oc}), low fill factor (FF) and short-circuit current density (J_{sc}). This bad performance can be very likely attributed to the so-called Fermi level pinning (FLP) at the semiconductor/metal junction. By contrast, a thin PEI interlayer results in higher FF and J_{sc} values with an extensive V_{oc} increase of almost 270 mV. On the one hand, the FF and J_{sc} improvement is consistent with the low contact resistance and passivation effect of PEI evidenced in TLMs and QSSPC experiments. On the other hand, the V_{oc} difference could be explained by the passivation and elimination of FLP and interface energy barriers. Use of a thin film of intrinsic amorphous silicon as an interlayer between the silicon and the polymer results in a 2% improvement of the FF maintaining similar V_{oc} and J_{sc} values. In this case, the excellent passivation of a-Si:H could promote electron accumulation at the interface

for a further improvement of the contact quality. Overall, a conversion efficiency up to 14.2% could be achieved in dopant-free silicon solar cells with selective contacts.
The dopant-free structures do not provide as good passivation as traditional HIT structures using doped a-Si:H layers. Therefore, we also studied the incorporation of PEI interlayers in classical ETL structures with n-doped a-Si:H. The FF value is once again improved by about 2%. This shows the potential of conjugated polyelectrolytes and particularly PEI to improve the contact even for optimized heterojunctions based on doped a-Si:H layers. In general terms the results on the photovoltaic devices agree with TLM experiments in the sense that PEI reduces the specific contact resistance, thereby reducing the series resistance of the solar cells. This can be seen in the consistent improvement of the FF of all the solar cells when PEI was incorporated to the rear contact.

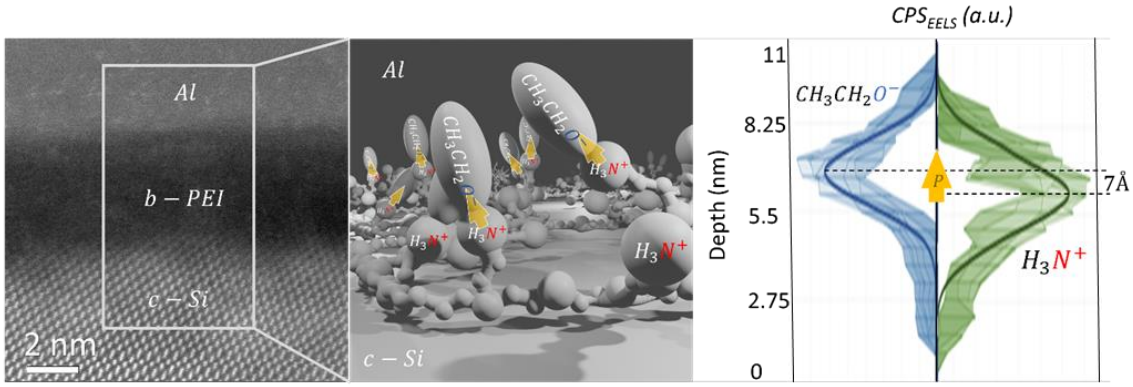

Fig (7)- Original scanning HRTEM image with 3D schematic of counterion condensation at PEI branches and a possible correlation with EELS compositional results and origin of the dipole potential.

Table (1) – PEI Solar cells summary of photovoltaic parameters

	FF (%)	V_{oc} (mV)	J_{sc} (mA/cm$_2$)	PCE (%)
c-Si/Al	64.38	339.8	28.30	6.19
c-Si/PEI/Al	72.12	606.7	31.50	13.70
c-Si/a-Si:H(i)/PEI/Al	74.78	601.5	31.63	14.20
c-Si/a-Si:H(i/n)/Al	71.75	668.2	32.56	15.64
c-Si/a-Si:H(i/n)/PEI/Al	73.62	662.9	32.79	16.01

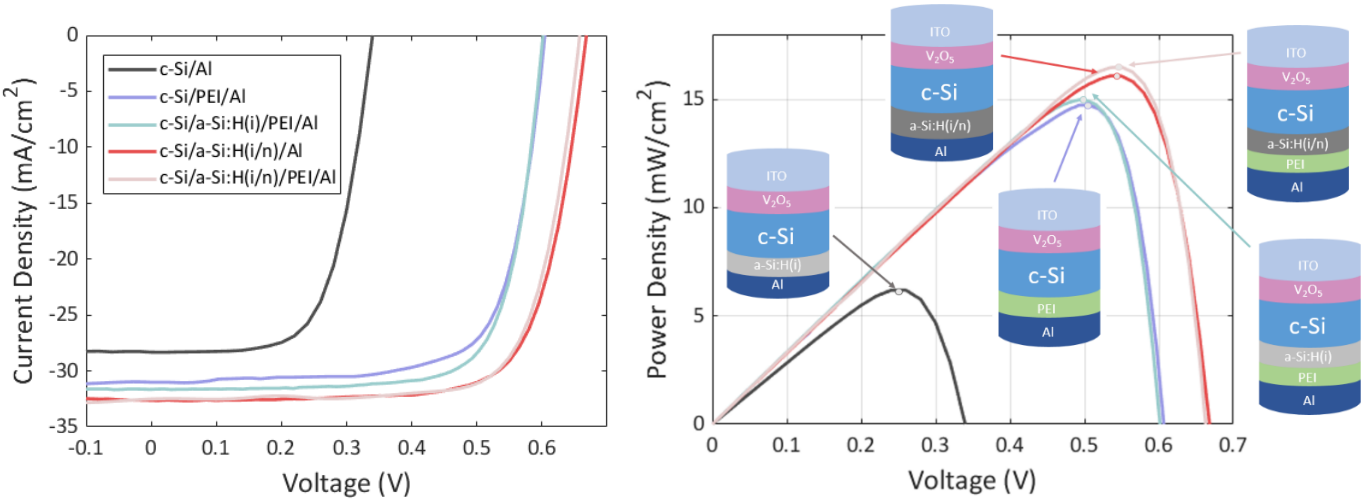

Fig (8)- Illuminated solar cells current voltage curve and output power density.

Conclusions

In this work, we have used branched polyethylenamine as a polymeric selective contact in crystalline silicon Metal/Insulator/Semiconductor junctions. According to TLM measurments, the contact resistance is optimum for a PEI layer thickness around 1 nm. QSSPC measurements for that optimized thickness show that the passivation of crystalline silicon improves after the metal is deposited. This suggests a charge transfer from the metal with consequent electron accumulation at the silicon surface. UPS results evidence that PEI can shift the electrode work function by approximately 1 eV. This effect is further enhanced by the using lower pkA solvents such as methanol. XPS results indicate that the amine groups present in the polymer are partially protonated due to the presence of N^+ signal in the nitrogen spectrum. The shift of work function measured by UPS is consistent with the pkA of the solvent, which has influence in the protonation of amine groups. Moreover, the presence of C-O and C=O bonds in XPS spectra may be related to leftover solvent in the polymeric film. This effect could be related to counter anion condensation in either ethanol, ethanolate or ethaldehyde forms. Compositional analysis with high spatial resolution in EELS measurements suggests gaussian profiles of oxygen and nitrogen within a mean distance of 7 Å. Nitrogen atoms are partially protonated and also part of the oxygen atoms are in the form of ionic ethanolate counter anions. The two-dimensional extension of these atoms implies a relatively ordered layer of strong interfacial dipoles as illustrated in Fig(7). The order in the layer may be promoted by chemical interaction with the substrate and the metallic contact. QSSPC measurements evidence a clear enhancement of surface passivation after the metal deposition accompanied by some additional shift of work function in UPS spectra. This leads us to conclude that the PEI modification induces an important charge transfer from the aluminium contact to the silicon substrate. At the same time, electron accumulation favours the transport of electrical current and reduces the specific contact resistance.

Finally, a series of solar cell structures have been fabricated to test the use of PEI in electron selective contacts. Full dopant-free solar cells with 14.2% efficiency have been demonstrated

with PEI modification at the contact. In solar cells with n-doped a-Si:H layer, the use of PEI at the interface increased the conversion efficiency 16%. Both cases show a clearly improved performance with respect to reference structures without the polymer. The consistently improved FF values can be explained by an important reduction of the contact resistance and the elimination of energy barriers from undesired Fermi level pinning.

Acknowledgements

This research has been supported by the Spanish government through Grants PID2019-109215RB-C41, PID2019-109215RB-C43, PID2020-115719RB-C21, PID2020-116719RB-C41 and funded by MCIN/AEI/ 10.13039/501100011033. Besides this the authors would like to thank prof. Jordi LLorca for his expertise and helpful discussions over XPS results, as well as Dr Rodrigo Fernández-Pacheco of the Laboratorio de Microscopias Avanzadas (LMA-INA) of Zaragoza for the HRTEM images EDS and EELS analysis, and Guillaume Sauthier from ICN2 for his contribution through UPS measurements and discussions.

In suporting information one can find AFM roughness characterization, Quasi Steady state Photo conductance lifetime curves and reference XPS spectra sample.

References

(1) Wan, L.; Zhang, C.; Ge, K.; Yang, X.; Li, F.; Yan, W.; Xu, Z.; Yang, L.; Xu, Y.; Song, D.; Chen, J. Conductive Hole-Selective Passivating Contacts for Crystalline Silicon Solar Cells. *Advanced Energy Materials* **2020**, *10* (16), 1–8. https://doi.org/10.1002/aenm.201903851.

(2) Allen, T. G.; Bullock, J.; Yang, X.; Javey, A.; De Wolf, S. Passivating Contacts for Crystalline Silicon Solar Cells. *Nature Energy* **2019**, *4* (11), 914–928. https://doi.org/10.1038/s41560-019-0463-6.

(3) Gao, P.; Yang, Z.; He, J.; Yu, J.; Liu, P.; Zhu, J.; Ge, Z.; Ye, J. Dopant-Free and Carrier-Selective Heterocontacts for Silicon Solar Cells: Recent Advances and Perspectives. *Advanced Science* **2018**, *5* (3). https://doi.org/10.1002/advs.201700547.

(4) Zhang, T.; Iqbal, S.; Zhang, X. Y.; Wu, W.; Su, D.; Zhou, H. L. Recent Advances in Highly Efficient Organic-Silicon Hybrid Solar Cells. *Solar Energy Materials and Solar Cells* **2020**, *204* (September 2019), 110245. https://doi.org/10.1016/j.solmat.2019.110245.

(5) Gerling, L. G.; Mahato, S.; Morales-Vilches, A.; Masmitja, G.; Ortega, P.; Voz, C.; Alcubilla, R.; Puigdollers, J. Transition Metal Oxides as Hole-Selective Contacts in Silicon Heterojunctions Solar Cells. *Solar Energy Materials and Solar Cells* **2016**, *145* (September), 109–115. https://doi.org/10.1016/j.solmat.2015.08.028.

(6) Yu, J.; Yu, J.; Yu, J.; Phang, P.; Samundsett, C.; Basnet, R.; Neupan, G. P.; Yang, X.; Macdonald, D. H.; Wan, Y.; Yan, D.; Ye, J. Titanium Nitride Electron-Conductive Contact for Silicon Solar Cells by Radio Frequency Sputtering from a TiN Target. *ACS Applied*

Materials and Interfaces **2020**, *12* (23), 26177–26183. https://doi.org/10.1021/acsami.0c04439.

(7) Wan, Y.; Samundsett, C.; Bullock, J.; Allen, T.; Hettick, M.; Yan, D.; Zheng, P.; Zhang, X.; Cui, J.; McKeon, J.; Javey, A.; Cuevas, A. Magnesium Fluoride Electron-Selective Contacts for Crystalline Silicon Solar Cells. *ACS Applied Materials and Interfaces* **2016**, *8* (23), 14671–14677. https://doi.org/10.1021/acsami.6b03599.

(8) Bullock, J.; Zheng, P.; Jeangros, Q.; Tosun, M.; Hettick, M.; Sutter-Fella, C. M.; Wan, Y.; Allen, T.; Yan, D.; Macdonald, D.; De Wolf, S.; Hessler-Wyser, A.; Cuevas, A.; Javey, A. Lithium Fluoride Based Electron Contacts for High Efficiency N-Type Crystalline Silicon Solar Cells. *Advanced Energy Materials* **2016**, *6* (14), 1–7. https://doi.org/10.1002/aenm.201600241.

(9) Wang, D.; Sheng, J.; Wu, S.; Zhu, J.; Chen, S.; Gao, P.; Ye, J. Tuning Back Contact Property via Artificial Interface Dipoles in Si/Organic Hybrid Solar Cells. *Applied Physics Letters* **2016**, *109* (4). https://doi.org/10.1063/1.4959839.

(10) Liu, J.; Ji, Y.; Liu, Y.; Xia, Z.; Han, Y.; Li, Y.; Sun, B. Doping-Free Asymmetrical Silicon Heterocontact Achieved by Integrating Conjugated Molecules for High Efficient Solar Cell. *Advanced Energy Materials* **2017**, *7* (19), 1–7. https://doi.org/10.1002/aenm.201700311.

(11) Battaglia, C.; Cuevas, A.; De Wolf, S. High-Efficiency Crystalline Silicon Solar Cells: Status and Perspectives. *Energy and Environmental Science* **2016**, *9* (5), 1552–1576. https://doi.org/10.1039/c5ee03380b.

(12) Adachi, D.; Hernández, J. L.; Yamamoto, K. Impact of Carrier Recombination on Fill Factor for Large Area Heterojunction Crystalline Silicon Solar Cell with 25.1% Efficiency. *Applied Physics Letters* **2015**, *107* (23), 22–25. https://doi.org/10.1063/1.4937224.

(13) VDMA. International Technology Roadmap for Photovoltaic. *International Technology Roadmap for Photovoltaic* **2018**, 76.

(14) Yang, X.; Xu, H.; Liu, W.; Bi, Q.; Xu, L.; Kang, J.; Hedhili, M. N.; Sun, B.; Zhang, X.; De Wolf, S. Atomic Layer Deposition of Vanadium Oxide as Hole-Selective Contact for Crystalline Silicon Solar Cells. *Advanced Electronic Materials* **2020**, *6* (8), 1–8. https://doi.org/10.1002/aelm.202000467.

(15) Tom, T.; Ros, E.; López-Pintó, N.; Miguel Asensi, J.; Andreu, J.; Bertomeu, J.; Puigdollers, J.; Voz, C. Influence of Co-Sputtered Ag:Al Ultra-Thin Layers in Transparent V2O5/Ag:Al/AZO Hole-Selective Electrodes for Silicon Solar Cells. *Materials* **2020**, *13* (21), 4905. https://doi.org/10.3390/ma13214905.

(16) He, L.; Jiang, C.; Wang, H.; Lai, D.; Rusli. High Efficiency Planar Si/Organic Heterojunction Hybrid Solar Cells. *Applied Physics Letters* **2012**, *100* (7), 1–4. https://doi.org/10.1063/1.3684872.

(17) Ratcliff, E. L.; Zacher, B.; Armstrong, N. R. Selective Interlayers and Contacts in Organic Photovoltaic Cells. *Journal of Physical Chemistry Letters* **2011**, *2* (11), 1337–1350. https://doi.org/10.1021/jz2002259.

(18) Chen, L.; Chen, Q.; Wang, C.; Li, Y. Interfacial Dipole in Organic and Perovskite Solar Cells. *Journal of the American Chemical Society* **2020**, *142* (43), 18281–18292. https://doi.org/10.1021/jacs.0c07439.

(19) Yan, L.; Song, Y.; Zhou, Y.; Song, B.; Li, Y. Effect of PEI Cathode Interlayer on Work Function and Interface Resistance of ITO Electrode in the Inverted Polymer Solar Cells. *Organic Electronics* **2015**, *17*, 94–101. https://doi.org/10.1016/j.orgel.2014.11.023.

(20) Ros, E.; Barquera, Z.; Ortega, P. R.; Gerling, L. G.; Masmitjà, G.; Martín, I.; Alcubilla, R.; Puigdollers, J.; Voz, C. Improved Electron Selectivity in Silicon Solar Cells by Cathode Modification with a Dipolar Conjugated Polyelectrolyte Interlayer. *ACS Applied Energy Materials* **2019**, *2* (8), 5954–5959. https://doi.org/10.1021/acsaem.9b01055.

(21) Reichel, C.; Würfel, U.; Winkler, K.; Schleiermacher, H. F.; Kohlstädt, M.; Unmüssig, M.; Messmer, C. A.; Hermle, M.; Glunz, S. W. Electron-Selective Contacts via Ultra-Thin Organic Interface Dipoles for Silicon Organic Heterojunction Solar Cells. *Journal of Applied Physics* **2018**, *123* (2). https://doi.org/10.1063/1.5010937.

(22) Ikeda, N.; Koganezawa, T.; Kajiya, D.; Saitow, K. I. Performance of Si/PEDOT:PSS Hybrid Solar Cell Controlled by PEDOT:PSS Film Nanostructure. *Journal of Physical Chemistry C* **2016**, *120* (34), 19043–19048. https://doi.org/10.1021/acs.jpcc.6b07101.

(23) Li, L. Y.; Chen, C. H.; Chiu, C. L.; Li, Y. L.; Meng, H. F.; Yu, P. Diffusion-Free Organic Hole Selective Contacts for Silicon Solar Cells. *Conference Record of the IEEE Photovoltaic Specialists Conference* **2019**, 2299–2302. https://doi.org/10.1109/PVSC40753.2019.8981369.

(24) Liu, P. H.; Chuang, C. H.; Zhou, Y. L.; Wang, S. H.; Jeng, R. J.; Rwei, S. P.; Liau, W. Bin; Wang, L. Conjugated Polyelectrolytes as Promising Hole Transport Materials for Inverted Perovskite Solar Cells: Effect of Ionic Groups. *Journal of Materials Chemistry A* **2020**, *8* (47), 25173–25177. https://doi.org/10.1039/d0ta09063h.

(25) Zhang, Z.; Yates, J. T. Band Bending in Semiconductors: Chemical and Physical Consequences at Surfaces and Interfaces. *Chemical Reviews* **2012**, *112* (10), 5520–5551. https://doi.org/10.1021/cr3000626.

(26) Agrawal, A.; Lin, J.; Barth, M.; White, R.; Zheng, B.; Chopra, S.; Gupta, S.; Wang, K.; Gelatos, J.; Mohney, S. E.; Datta, S. Fermi Level Depinning and Contact Resistivity Reduction Using a Reduced Titania Interlayer in N-Silicon Metal-Insulator-Semiconductor Ohmic Contacts. *Applied Physics Letters* **2014**, *104* (11). https://doi.org/10.1063/1.4868302.

(27) Ji, W.; Allen, T.; Yang, X.; Zeng, G.; De Wolf, S.; Javey, A. Polymeric Electron-Selective Contact for Crystalline Silicon Solar Cells with an Efficiency Exceeding 19%. *ACS Energy Letters* **2020**, *5* (3), 897–902. https://doi.org/10.1021/acsenergylett.0c00110.

(28) Yang, X.; Ying, Z.; Yang, Z.; Xu, J.; Wang, W.; Wang, J.; Wang, Z. Light-Promoted Electrostatic Adsorption of High-Density Lewis Base Monolayers as Passivating Electron-Selective Contacts. **2020**, *2003245*, 1–13. https://doi.org/10.1002/advs.202003245.

(29) Wan, Y.; Samundsett, C.; Bullock, J.; Allen, T.; Hettick, M.; Yan, D.; Zheng, P.; Zhang, X.; Cui, J.; McKeon, J.; Javey, A.; Cuevas, A. Magnesium Fluoride Electron-Selective

Contacts for Crystalline Silicon Solar Cells. *ACS Applied Materials and Interfaces* **2016**, *8* (23), 14671–14677. https://doi.org/10.1021/acsami.6b03599.

(30) Manning, G. S. Limiting Laws and Counterion Condensation in Polyelectrolyte Solutions. 7. Electrophoretic Mobility and Conductance. *Journal of Physical Chemistry* **1981**, *85* (11), 1506–1515. https://doi.org/10.1021/j150611a011.

(31) Chen, L.; Chen, Q.; Wang, C.; Li, Y. Interfacial Dipole in Organic and Perovskite Solar Cells. *Journal of the American Chemical Society* **2020**, *142* (43), 18281–18292. https://doi.org/10.1021/jacs.0c07439.

(32) Perlich, J.; Körstgens, V.; Metwalli, E.; Schulz, L.; Georgii, R.; Müller-Buschbaum, P. Solvent Content in Thin Spin-Coated Polystyrene Homopolymer Films. *Macromolecules* **2009**, *42* (1), 337–344. https://doi.org/10.1021/ma801878j.

(33) García-Turiel, J.; Jérôme, B. Solvent Retention in Thin Polymer Films Studied by Gas Chromatography. *Colloid and Polymer Science* **2007**, *285* (14), 1617–1623. https://doi.org/10.1007/s00396-007-1733-6.

(34) Wang, C.; Luo, Y.; Zheng, J.; Liu, L.; Xie, Z.; Huang, F.; Yang, B.; Ma, Y. Spontaneous Interfacial Dipole Orientation Effect of Acetic Acid Solubilized PFN. *ACS Applied Materials and Interfaces* **2018**, *10* (12), 10270–10279. https://doi.org/10.1021/acsami.8b00975.

(35) Masmitjà, G.; Gerling, L. G.; Ortega, P.; Puigdollers, J.; Martín, I.; Voz, C.; Alcubilla, R. V2O: X-Based Hole-Selective Contacts for c-Si Interdigitated Back-Contacted Solar Cells. *Journal of Materials Chemistry A* **2017**, *5* (19), 9182–9189. https://doi.org/10.1039/c7ta01959a.

Table of content graphic

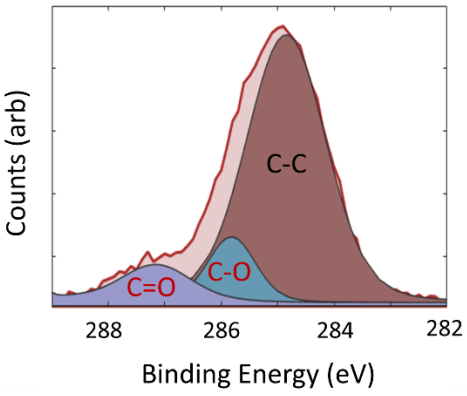

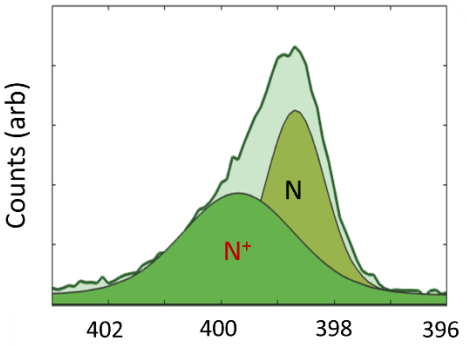

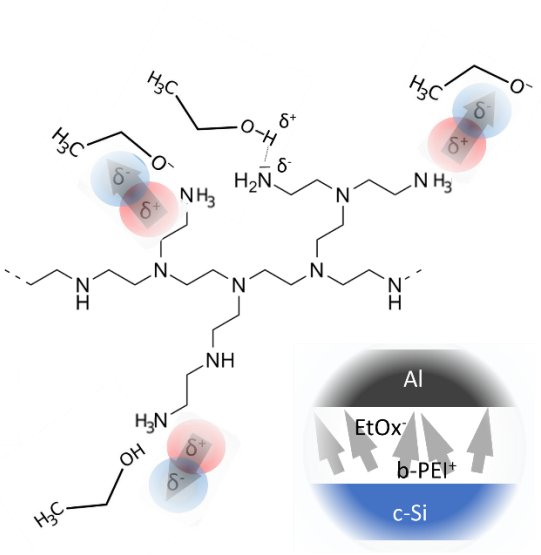

$$C2H5{-}OH + NH2{-}R \rightarrow C2H5O + NH3{-}R$$